

## The Effect of Applied Stress on the Crevice Corrosion of P110 Steel in Simulated Oilfield Produced Water

Zhang Ying<sup>1</sup>, Yang kun<sup>1,\*</sup>, Yu liusi<sup>2</sup>, GAO anqi<sup>1</sup>

<sup>1</sup> College of Mechanical Engineering, Sichuan University of Science & Engineering, Zigong 643000, China;

<sup>2</sup> College of Materials Science and Engineering, Sichuan University of Science & Engineering, Zigong 643000, China;

\*E-mail: [1822684313@qq.com](mailto:1822684313@qq.com)

Received: 1 June 2022/ Accepted: 2 August 2022/ Published: 10 September 2022

---

The effect of applied stress on the crevice corrosion of P110 well pipe thread joint steel was investigated using electrochemical measurements and surface analysis technologies in simulated oil and gas field solutions. The results show obvious crevice corrosion on the surface of P110 steel after 12 h of immersion in a simulated solution with the coexistence of crevice stress. The applied stress made the corrosion potential of P110 steel shift in a more negative direction, which indicates that the crevice corrosion tendency of P110 steel increased due to the applied stress, and the corresponding corrosion rate was accelerated. This behavior may be ascribed to the stress destroying the compactness of corrosion products and reducing the barrier effect of corrosion products.

---

**Keywords:** P110 steel, crevice corrosion, stress, electrochemistry

### 1. INTRODUCTION

As one of the important infrastructures of oil and gas fields, an oil well pipe transports oil and gas from underground to the ground. Ensuring the stable and safe operation of oil well pipes is the basic requirement of exploiting oil and gas fields. As shown in Fig. 1, well pipes are usually threaded underground with couplings and form thousands of meters of pipe posts. Gaps inevitably form at the threaded connection between the well pipe fittings and the couplings. When the interconnecting oil well pipe is corroded in the oil and gas field environment, the corrosive medium will infiltrate into the crevice of the thread connection over time. The small crevice hinders the mass transfer process of the corrosive medium, which results in a difference in the chemical composition of the corrosive medium inside and outside the crevice; thus, crevice corrosion easily occurs [1]. In addition, the stress generated by the gravity of the oil well pipe will affect the thread connection, and the corrosion sensitivity of the thread connection of the oil well pipe joint may increase. Once the corrosive behavior of the well pipe destroys

the joint and coupling thread structure, the failure of the thread sealing surface will make the oil well pipe connection leak, so the oil well pipe connection will no longer be able to withstand the existing huge stress, which causes the fracture and scrapping of the oil well pipe and the occurrence of major accidents in oil and gas fields. Therefore, crevice and stress are important factors that cause serious corrosion in the joint of oil well pipe threads.

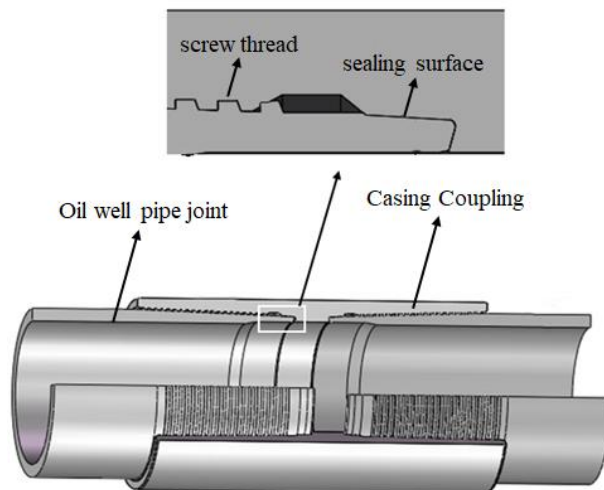


**Figure 1.** Schematic diagram of an oil well pipe connection

Crevice corrosion is a common form of local corrosion regardless of the environment; as long as there are crevices between metals or components, crevice corrosion may occur, which results in local defects on the metal surface. Song, Guo[2-3] and other researchers think that  $\text{Cl}^-$  has a very important influence on the corrosion behavior of metals; its strong penetrability is ascribed to its small radius, and the hydrolysis of corresponding chlorides decreases the pH values and promotes the crevice corrosion rate. In other words, the susceptibility of crevice corrosion is increased by  $\text{Cl}^-$ . Lee et al.[4] found that the increase in  $\text{Cl}^-$  acidified the corrosive medium by studying the crevice corrosion of carbon steel, which accelerated the development of crevice corrosion. Stress corrosion refers to the local corrosion damage caused by tensile stress far lower than the yield strength of the material for some time in a corrosive medium[5]. Stress and corrosive medium are common factors of stress corrosion. The increase in stress will promote the occurrence of stress corrosion cracking. Longkui et al.[6] found that ultralow elastic stress could form microcracks on the pitting shoulder and accelerate the occurrence of stress corrosion. Hahm et al.[7] found that the electrochemical activity of the material increased with increasing applied stress. Tang[8] studied the influence of stress on the local anodic dissolution of materials by microelectrochemistry and found that applied stress accelerated the anodic dissolution of materials. Some studies have suggested that[9-10] stress concentrations are generated at metal defects and lead to stress corrosion cracking, and crevice corrosion can cause defects on metal surfaces, so local defects produced by crevice corrosion may be the source of crack germination, which makes metal stress corrosion more sensitive. Turnbull et al.[11] found that pitting was the main cause of stress corrosion cracking of materials in corrosive media containing  $\text{Cl}^-$ . Zhu et al.[12] found that pitting could

concentrate applied stress on materials. With the expansion of pits, the stress concentration became more obvious, so stress corrosion cracking of materials occurred. In addition, stress can affect the local corrosion of metals. Lu, B. T et al[13] found that stress reduced the stability of the passivated film structure and increased the local corrosion sensitivity of the metal. G.A. Zhang et al.[14] have shown that applied stress increased the defect of the metal passivation film and promoted the local corrosion of the metal.

In summary, the current research on metal crevices and stress corrosion behavior is mainly concentrated on considering a single factor, while the corrosion behavior of oil well pipes is more complex when crevices and stress coexist, and there are few related studies. This paper will study the corrosion behavior of P110 well pipe steel under coupled crevice-stress conditions through electrochemical measurements and microscopic analysis, discuss the corrosion mechanism of P110 oil well pipe steel under coupled crevice-stress conditions, and provide a certain theoretical reference for the safe service of P110 well pipes in oil and gas fields.

## 2. EXPERIMENT

### 2.1 Material

The material in this experiment is P110 oil well pipe steel. The chemical composition is shown in Table 1.

**Table 1.** Chemical composition of P110 steel (wt.%)

Steel	C	Si	P	Mn	Ni	Cr	Mn	Fe
P110	0.28%	0.25%	0.013%	1.141%	0.024%	0.05%	0.03%	margin

The tensile specimen of P110 steel was prepared according to GB/T 15970. The stress–strain curve of P110 steel was measured by a tensile testing machine. The applied stress was chosen according to the stress–strain curve.

### 2.2 Electrochemical measurements

To mimic the actual working conditions, the test solution was simulated according to the typical oilfield produced water. The chemical composition was 17.458 g/L NaCl, 1.143 g/L CaCl<sub>2</sub>, 0.863 g/L MgCl<sub>2</sub>·6H<sub>2</sub>O, and 980.206 g/L H<sub>2</sub>O. All tests were performed at 25 °C and normal pressure.

A three-electrode system was used to study the electrochemical corrosion behavior of P110 steel. A saturated calomel electrode (SCE) was used as the reference electrode, a platinum electrode was used as the counter electrode, and a P110 plate was used as the work electrode. The open circuit potential

(OCP) was monitored during the immersion process; then, electrochemical impedance spectroscopy (EIS) was performed at the open circuit potential. The corresponding frequency ranged from  $10^5$  Hz to  $10^2$  Hz, and the amplitude was 5 mV. Finally, the potentiodynamic polarization curve was measured from -0.2 V to 1 V relative to the open circuit potential, and the scanning rate was 0.5 mV/s. All potentials in this paper are relative to SCE.

### 2.3 Surface morphology analysis

After the polarization curve measurement, the corrosion morphology of P110 steel was characterized by scanning electron microscopy (SEM), and the chemical composition was analyzed by coupled energy disperse spectroscopy (EDS).

### 2.4 Experimental apparatus

The size of the P110 steel sample in this crevice-stress coupling experiment is 150 mm×50 mm×1 mm. Before the test, the samples were successively polished with sandpaper (500#-2000#) until their surfaces were smooth and cleaned with n-hexane, alcohol, and deionized water.

To achieve a good electric connection with the electrochemical workstation, the end of the sample was connected to a copper wire. Except for the working area of 20 mm×10 mm in the center part, the remaining part was sealed with sealant. After the sealant solidified, a four-point bending stress loading method was used to quantitatively load the stress of the sample, as shown in Fig. 2.

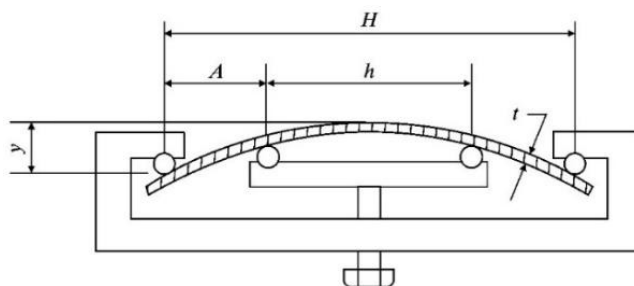


**Figure 2.** Schematic diagram of the four-point bending loading device

The tensile stress was applied to the sample by rotating the bottom bolt, and the calculation method of the specific value of the stress is as follows[15]:

$$\delta = \frac{12Ety}{3H^2 - 4A^2} \quad (1)$$

where:  $\delta$ —maximum tensile stress, MPa

E—Elastic modulus, MPa

t—Sample thickness, mm

y—Maximum deflection between two external supports, mm

A—Distance between inner and outer supports, mm

Fig. 3(a) shows the electrochemical corrosion device of P110 steel under the condition of coexisting crevice stress. A three-electrode system was adopted in the experiment, and copper wires welded to the P110 steel plate were connected to the working electrode. Only a 2-cm<sup>2</sup> work area was retained in the middle part of the sample, in which 1 cm<sup>2</sup> was simulated inside the crevice, and 1 cm<sup>2</sup> was simulated outside the crevice. The salt bridge with porous ceramics at the bottom and platinum electrode were encapsulated with epoxy resin, as shown in Fig. 3(b), and the reference electrode was inserted into the salt bridge. The encapsulated salt bridge and platinum electrode were placed on top of the sample to act as a cover plate to create gaps and measure the electrochemical reactions in the gaps of the sample. A 300- $\mu$ m-thick PTFE spacer was placed between the encapsulated electrode and the sample to simulate the crevice. In addition, for the accuracy of the experiment, instead of the traditional saturated KCl solution, the test solution was injected into the salt bridge.

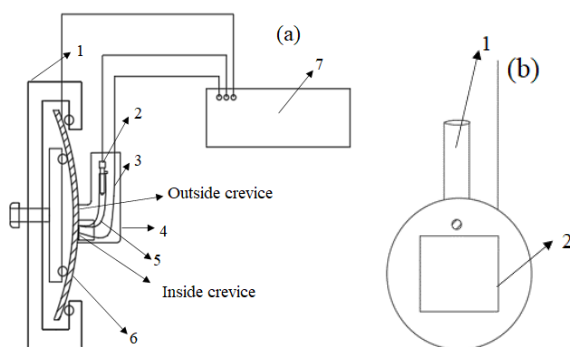


**Figure 3.** (a) P110 electrochemical measuring device under coexisting stress and crevice conditions (1. four-point bending loading device; 2. reference electrode; 3. platinum electrode; 4. L shaped acrylic tube; 5. salt bridge; 6. P110 steel; 7. electrochemical workstation); (b) crevice cover sheet (1. salt bridge; 2. platinum electrode)

### 3. RESULTS AND DISCUSSION

#### 3.1 Stress–strain curve

Fig. 4 shows the stress–strain curve of P110 steel. The yield strength and elastic modulus of P110 steel are 804 MPa and 206 MPa, respectively. To highlight the difference in the test, stresses of 200 MPa, 400 MPa, and 600 MPa were applied to the samples.

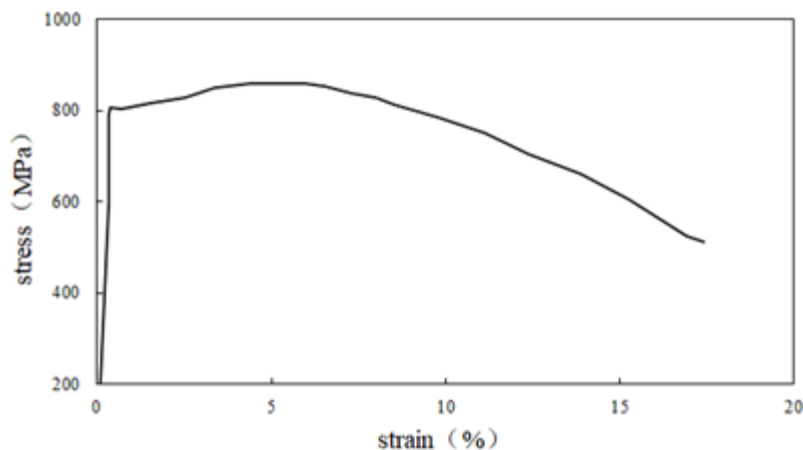


**Figure 4.** Stress-strain curve of P110 steel in the air

### 3.2 Open circuit potential

The open circuit potential of P110 steel in the simulated solution was monitored during 12 h of immersion under different stress states, and the OCP values are shown in Fig. 5. In Fig. 5, whether inside or outside the crevice, the corrosion potential of P110 steel had the same trend over time: it rapidly decreased within 1 h of immersion and gradually remained relatively stable, and the open circuit potential measured outside the crevice was always higher than that measured inside the crevice. J.Mu[16] et al. found that the inhibition of the cathode reaction in the crevice resulted in the decrease of the open circuit potential potential in the crevice. Therefore, the P110 steel inside the crevice was the anode, but that outside the crevice was the cathode.

By comparison with Figs. 5(a) -(d) and focusing on the potential measured outside the crevice, we obtained the OCP value of -0.655 V without the stress, and it shifted to a more negative potential due to the applied stress. Finally, it remained at -0.673 V, -0.689 V, and -0.705 V for 200 MPa, 400 MPa, and 600 MPa after 12 h of immersion, respectively. That is the applied stress reduced the open circuit potential value of P110 steel in the simulated solution. Some studies[17-18] have shown that the applied stress reduces the stability of the passivation film on the surface of the metal, causing its open circuit potential to shift negatively, increasing the corrosion sensitivity of the metal. The same conclusion is obtained by analyzing the OCP measured inside the crevice. The OCP values under different states are summarized in Table 2, and the difference in potential inside and outside the crevice ( $\Delta E$ ) was calculated.

From Table 2,  $\Delta E$  increased with increasing applied stress; the greater the difference of open circuit potential inside and outside the crevice, the stronger the driving force of metal corrosion[19], which indicates that the driving force of crevice corrosion was enhanced by the increased stress. Therefore, the corrosion of P110 steel in the crevice was accelerated.

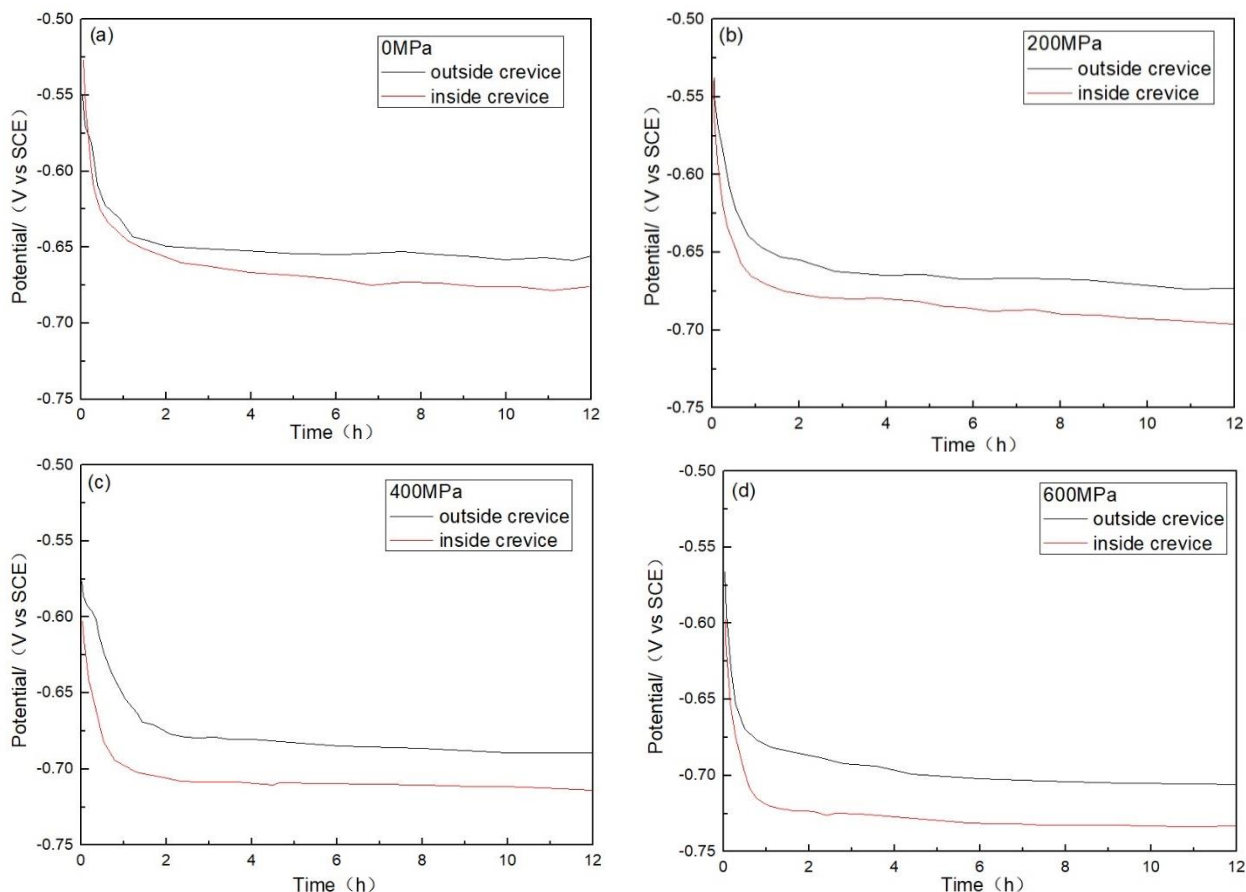


**Figure 5.** Open circuit potentials tendency inside and outside crevice of P110 steel during 12h of the immersed in simulated solution under different applied stress states (a).0MPa stress (b).200MPa stress (c).400MPa stress (d).600Mpa stress

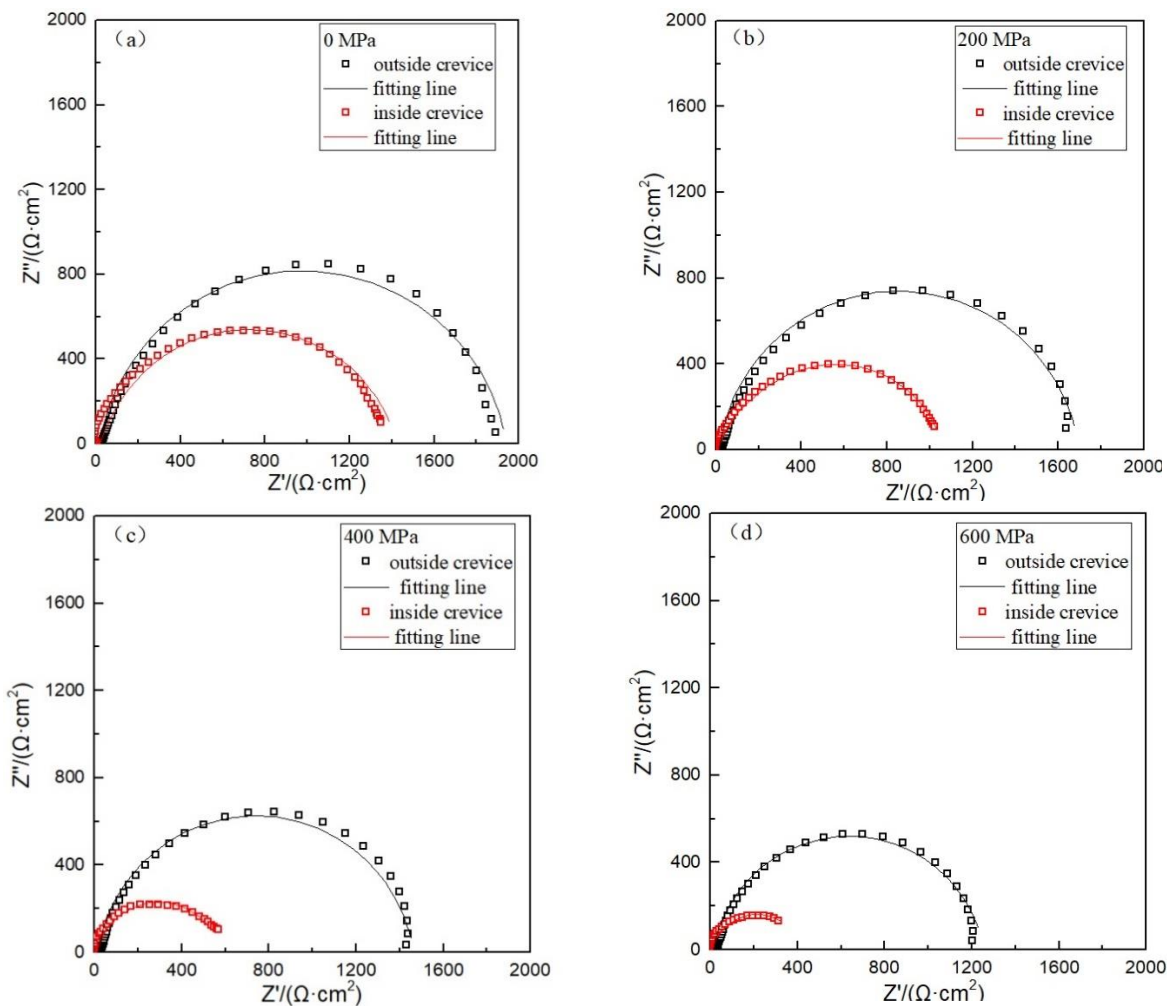
**Table 2.** The Open circuit potential outside and inside of crevice of P110 steel soaked in simulated solution for 12h under different applied stresses

Stress/MPa	$E_{inside}/V$	$E_{outside}/V$	$\Delta E/V$
0	-0.655	-0.675	0.020
200	-0.673	-0.696	0.023
400	-0.689	-0.713	0.024
600	-0.705	-0.732	0.027

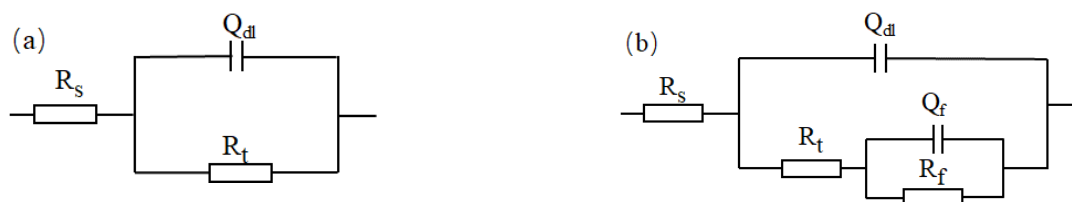
### 3.3 Electrochemical impedance spectroscopy

Fig. 6 shows the EIS diagrams of the P110 steel obtained inside and outside the crevice after 12 h of immersion in the simulated solution under different stresses. The Nyquist plots were composed of a part of the capacitive semicircle, in which the capacitive loop at high frequency may correspond to by the charge transfer resistance, and the capacitive loop at low frequency may be related to the corrosion products on the material surface[20], which indicates that the corrosion of P110 steel was activation-controlled in the simulated solution[21]. The corrosion rate of the metal in solution is inversely

proportional to the diameter of the capacitive semicircle; i.e., a smaller capacitive semicircle diameter corresponds to a faster corrosion rate of the metal[22]. In the Nyquist diagram under different applied stresses, the diameter of the capacitive loop in the crevice was apparently smaller than that outside the crevice, which should be caused by the rapid corrosion rate in the crevice and corrosion products on the surface of the crevice[23].



**Figure 6.** EIS diagram inside and outside the crevice of P110 steel soaked in the test solution for 12 h under different stresses: (a) 0MPa stress, Nyquist plots (c) 200MPa stress, Nyquist plots (e) 400MPa stress, Nyquist plots (g) 600MPa stress, Nyquist plots



**Figure 7.** Equivalent circuit model inside and outside crevice of P110 steel soaked in the test solution for 12h under different stress states: (a) outside the crevice and (b) inside the crevice

In addition, with the increase in applied stress, the capacitive loop diameter inside and outside the P110 steel crevice decreased to varying degrees, which indicates that the applied stress accelerated the corrosion behavior inside and outside the crevice[24].

Considering the applied stress, both inside and outside the crevice, the capacitive semicircle diameter of P110 steel showed an apparent decrease after the stress was applied, as shown in Figs. 6 (a) to (d), which indicates that the corrosion resistance of P110 steel deteriorated due to the applied stress. This is consistent with the previous reports[25-26], the applied stress increases the defects on the metal surface and makes the corrosion deteriorate further.

**Table 3.** The electrochemical impedance spectroscopy parameters for inside and outside of crevice of P110 steel immersed in simulated solution for 12h under different applied stresses

	Stress/MPa	$R_s/(\Omega \cdot \text{cm}^2)$	$Q_f/(\mu\text{F} \cdot \text{cm}^2)$	$n_f$	$R_f/(\Omega \cdot \text{cm}^2)$	$Q_{dl}/(\mu\text{F} \cdot \text{cm}^2)$	$n_{dl}$	$R_t/(\Omega \cdot \text{cm}^2)$
Outside the crevice	0	18.29				$1.86 \times 10^{-4}$	0.89	1923
	200	17.79				$5.34 \times 10^{-4}$	0.90	1627
	400	17.60				$3.21 \times 10^{-4}$	0.91	1445
	600	15.64				$4.81 \times 10^{-4}$	0.89	1239
Inside the crevice	0	17.61	$5.91 \times 10^{-5}$	0.80	1256	$8.78 \times 10^{-5}$	0.86	151
	200	14.83	$8.17 \times 10^{-4}$	0.79	649	$4.09 \times 10^{-4}$	0.91	402
	400	12.23	$9.83 \times 10^{-4}$	0.79	83	$3.77 \times 10^{-4}$	0.87	484
	600	10.52	$8.39 \times 10^{-4}$	0.73	21	$9.86 \times 10^{-4}$	0.88	388

To quantitatively analyze the effect of applied stress on the crevice corrosion of P110 steel in the simulated solution, the EIS data were fitted using the equivalent circuits[27] in Fig. 7, and the fitting results are shown in Table 3. where  $R_s$  is the solution resistance,  $Q_{dl}$  is the double-layer capacitance,  $n_{dl}$  is the double-layer capacitance index,  $R_t$  is the charge transfer resistance,  $Q_f$  is the capacitance of the corrosion products,  $n_f$  is the capacitance index of the corrosion products, and  $R_f$  is the corrosion product resistance. Different equivalent circuits were used to fit the EIS plots inside and outside the crevices. Fig. 7 (a) was used to fit the EIS data from the external surface, and Fig. 7 (b) was used to fit the EIS data from the inner crevice. This is ascribed to the fact that after 12 h of immersion, the oxygen differential cell was set between the crevice and the external surface due to restricted oxygen diffusion. The P110 steel outside the crevice was given a cathodic character, but the steel in the crevice was given an anodic character. This difference accelerated the corrosion rate of P110 steel in the crevice but inhibited that outside the crevice [28]. Hence, corrosion products were obviously observed in the crevice area.

Compared to the  $R_t$  value inside the crevice, that outside the crevice was always higher, which is attributed to the oxygen differential cell corrosion.  $R_t$  also decreased with increasing applied stress, which indicates the accelerating effect of applied stress on the corrosion rate.  $R_p$  is the polarization resistance in the entire reaction process ( $R_p = R_t + R_f$ ). The polarization resistance reflects the resistance of the entire electrochemical reaction process; i.e., a smaller  $R_p$  corresponds to a faster corrosion rate of the

metal[29-30]. Fig. 8 shows the  $R_p$  values of P110 steel inside and outside the crevice under different stress conditions. Under different applied stresses, the  $R_p$  values inside and outside the crevice showed identical trends.  $R_p$  inside the crevice was always lower than that outside the crevice, which shows that the presence of the crevice accelerated the corrosion rate of the metal, and with the increase in applied stress, the  $R_p$  values inside and outside the P110 steel crevice gradually decreased. Thus, the applied stress accelerates the corrosion rate and deteriorates the corrosion resistance of P110 [17]. In addition, compared with the outside of the crevices,  $R_p$  in the crevice more significantly dropped, which indicates that the impact of stress on the corrosion rate in the crevices was greater than that outside the crevices. According to the above analysis of the open circuit potential of P110 steel, it is known that the corrosion in the crevices of P110 steel is mainly controlled by the anodic reaction, and some articles[31-32] have confirmed the acceleration effect of tensile stress on the anodic reaction.

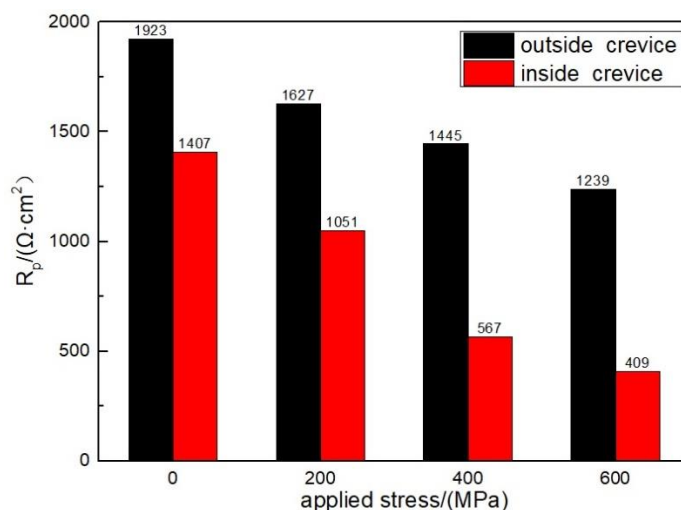


**Figure 8.**  $R_p$  values inside and outside crevice of P110 steel after immersed in simulated solution for 12h under different applied stresses states

### 3.4 Polarization curves

Fig. 9 shows the polarization curves of P110 steel inside and outside the crevice under different stresses after 12 h of immersion. Both cathodic and anodic reactions of P110 steel inside and outside the crevice were controlled by activation polarization, Bi[33] and Singh[34] et al. also found that P110 steel is in an activated and dissolved state under certain environments, without activating/passivation transition zone and passivation. The anodic current density quickly increased with increasing applied potential. Thus, the corrosion mechanism of P110 steel did not change with the applied stress. Compared with the outside of the crevice, repeated inflection points are observed in the polarization curve inside the crevice, and with the increase in applied stress, the amplitude of the inflection point increased, which may be related to the generation and destruction of metal surface corrosion products[35]. Almuaili et al.[36] found that stress can increase the dissolution rate of metal surface and accelerate the corrosion rate of metal. From Fig. 9, the polarization curves apparently negatively shifted to the right due to the

applied stress, which indicates that the corrosion rate was evidently accelerated by the increased applied stress.

The Tafel epitaxy method was used to fit the polarization curve, and the fitting data are shown in Table 4. From Table 4, the corrosion potential ( $E_{corr}$ ) in the crevice was always more negative than that outside the crevice, which indicates a higher corrosion tendency in the simulated solution. This result is consistent with the open circuit potential results. According to the polarization curve fitting data, with increasing applied stress, the corrosion potential gradually decreased. When there was no stress, the corrosion potential inside and outside the crevice of P110 steel was -0.646 V and -0.608 V, respectively. When the applied stress was 600 MPa, the corrosion potentials inside and outside the crevice were -0.749 V and -0.708 V, respectively. Bao et al.[37] also found that the corrosion current density of metal induced by tensile stress is higher than that without stress, author measured the corrosion current density of the overall surface of the metal and this experiment measured the corrosion current density of different parts of the surface of P110 steel metal.

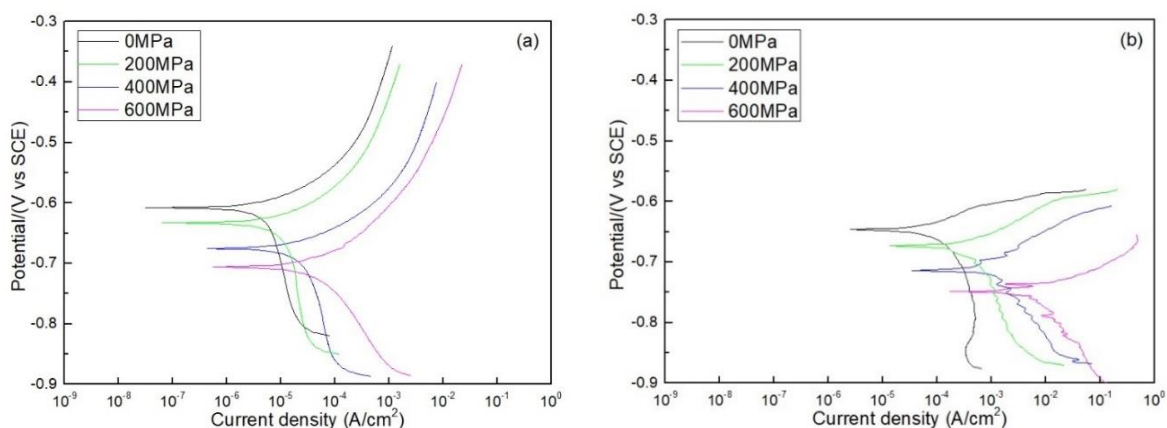


**Figure 9.** The internal and external of crevice polarization curves of P110 steel under different stress states after soaking the test solution for 12h (a) outside crevice (b) inside crevice

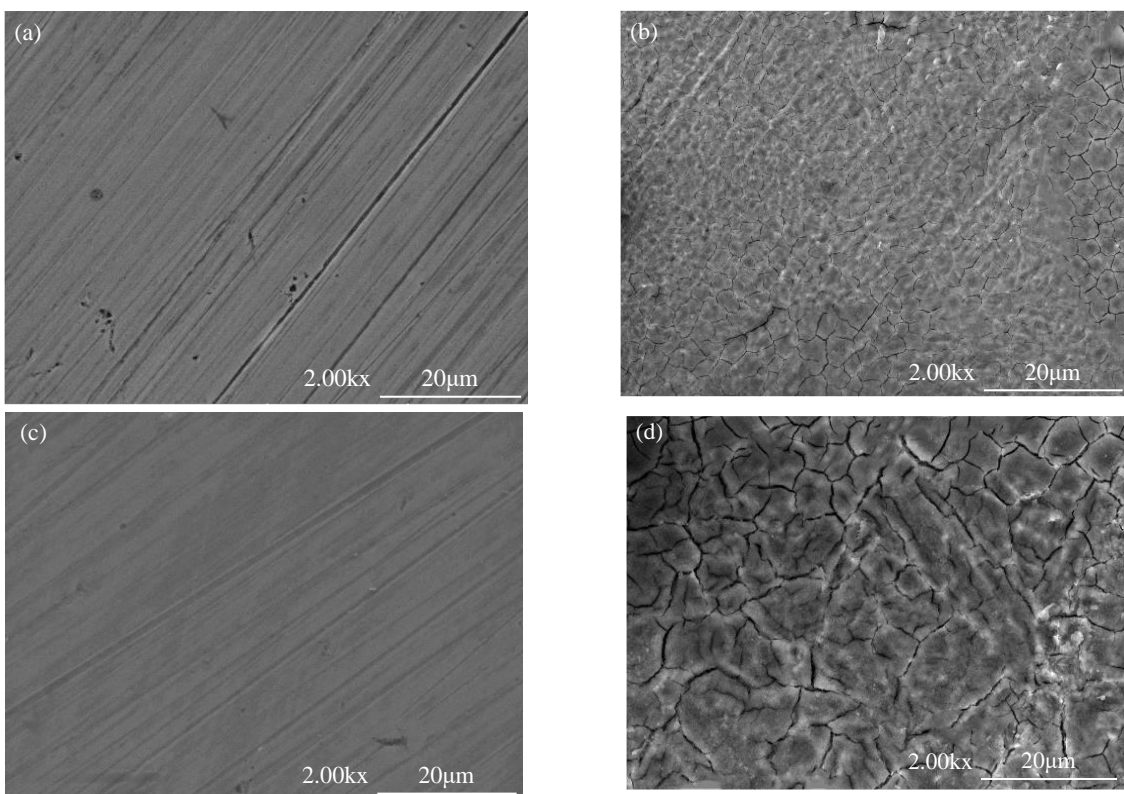
Under equal applied stress, the corrosion potential of P110 steel in the crevice was lower than the corrosion potential outside the crevice; with the increase in applied stress, the corrosion potential inside and outside the crevice was reduced to varying degrees, which indicates that the applied stress increased the corrosion tendency of P110 steel in the test solution. The corrosion rate of metal can be expressed by the corrosion current density. A smaller corrosion current density corresponds to a lower corrosion velocity of the metal [38]. When the applied stress was 0 MPa, the corrosion current densities inside and outside the crevices of P110 steel were  $1.55 \times 10^{-4} \text{ A}\cdot\text{cm}^{-2}$  and  $5.54 \times 10^{-6} \text{ A}\cdot\text{cm}^{-2}$ , respectively. When the applied stress was 600 MPa, the corrosion current densities inside and outside the crevices of P110 steel were  $4.40 \times 10^{-3} \text{ A}\cdot\text{cm}^{-2}$  and  $5.49 \times 10^{-5} \text{ A}\cdot\text{cm}^{-2}$ , respectively. The corrosion current density inside the crevice was higher than that outside the crevice. With the increase in applied stress, the corrosion current density inside and outside the crevice increased to varying degrees, but the corrosion current density inside the crevice remained higher than that outside the crevice. Thus, crevice corrosion

can occur in the simulated solution, the corrosion rate in the crevice is higher than that outside the crevice, and the corrosion current density inside and outside the crevice increases with increasing applied stress, which indicates that the applied stress shows a promotion effect on the corrosion behavior inside and outside the crevice.

**Table 4.** fitting parameters of polarization curves of inside and outside crevice of P110 steel after immersed in test solution for 12 h under different stress states

Stress/MPa	$E_{corr}/V(\text{outside})$	$E_{corr}/V(\text{inside})$	$I_{corr}/A \cdot \text{cm}^{-2}(\text{outside})$	$I_{corr}/A \cdot \text{cm}^{-2}(\text{inside})$
0	-0.608	-0.646	$5.54 \times 10^{-6}$	$1.55 \times 10^{-4}$
200	-0.634	-0.673	$1.21 \times 10^{-5}$	$5.47 \times 10^{-4}$
400	-0.675	-0.713	$2.78 \times 10^{-5}$	$1.11 \times 10^{-3}$
600	-0.706	-0.749	$5.49 \times 10^{-5}$	$4.40 \times 10^{-3}$

### 3.5 Surface morphology analysis



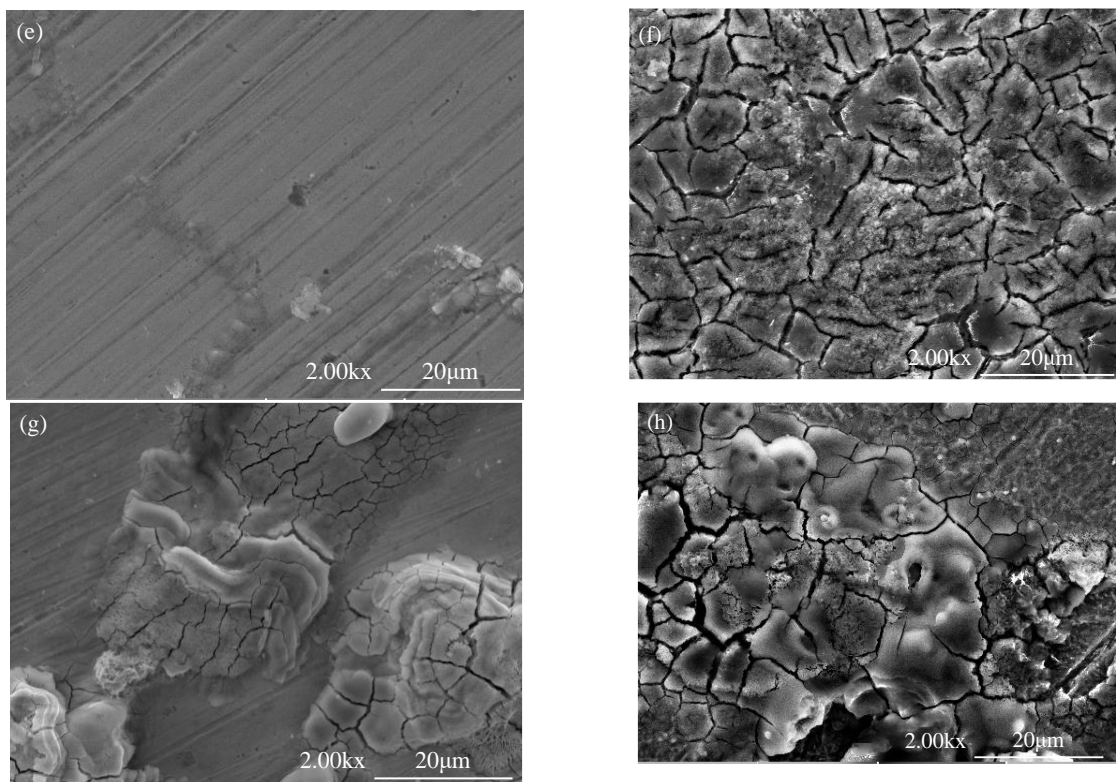


**Figure 10.** SEM images inside and outside the crevice of P110 steel under different applied stresses after 12 h of immersion in the simulated solution: (a) 0MPa stress outside crevice (b)0MPa stress inside crevice (c)200MPa stress outside crevice (d) 200MPa stress inside crevice (e) 400MPa stress outside crevice (f) 400MPa stress inside crevice (g) 600MPa stress outside crevice (h) 600MPa stress inside crevice

Although the effect of stress on the metal surface has been discussed in previous studies[39-40], the effect of stress on the inner and outer surfaces of the metal crevice was investigated in this experiment. Fig. 10 shows the surface morphology inside and outside the crevice of P110 steel under different applied stresses after 12 h of immersion in a simulated solution. The comparison between the inside and outside of the crevice shows that regardless of stress, more corrosion products were generated in the crevice, while the outer surface of the crevice was relatively smooth, and there were fewer corrosion products, which indicates that P110 steel suffered serious corrosion behavior in the crevice. Figs. 10(a) and 4(c) show that under the applied stress of 200 MPa, there is no obvious difference between the metal surface outside the crevice and that without stress, and there is no obvious corrosion on the outside surface of the crevice. However, with the increase in applied stress, at 400 MPa, as shown in Fig. 10 (e), slight corrosion traces and corrosion products appeared on the surface outside the crevice. At 600 MPa, as shown in Fig. 10 (g), the corrosion traces were more obvious. Compared with the corrosion surface obtained from the outside at 400 MPa, more corrosion products were observed at 600 MPa. Focusing on the inner surface of the crevice (Figs. 10b and d), a large quantity of corrosion products appeared on the inner surface of the crevice due to the applied stress (200 MPa), and the corrosion products obtained with applied stress were significantly looser than those obtained without stress. When the applied stress increased to 400 MPa and 600 MPa, the cracks of the corrosion products

in the crevice expanded again, which shows that the presence of applied stress formed more loose corrosion products in the crevice and destroyed the protective effect of the corrosion products on the metal matrix. The SEM images of P110 steel show a significant difference in crevice corrosion inside and outside the crevices. The corrosion outside the crevices was slight, while the corrosion inside the crevices was serious, and more corrosion products were produced. The existence of applied stress deteriorated the corrosion behavior inside and outside the crevice, which is consistent with the results of the electrochemical test.

### 3.5 EDS analysis

Fig. 11 and Table 5 show the EDS scanning area inside and outside the crevice and the specific EDS values after P110 steel had been soaked in the simulated solution for 12 h under stresses of 0 MPa and 400 MPa, respectively. As the table shows, with the increase in applied stress, the Fe element in the P110 steel crevice is significantly reduced.

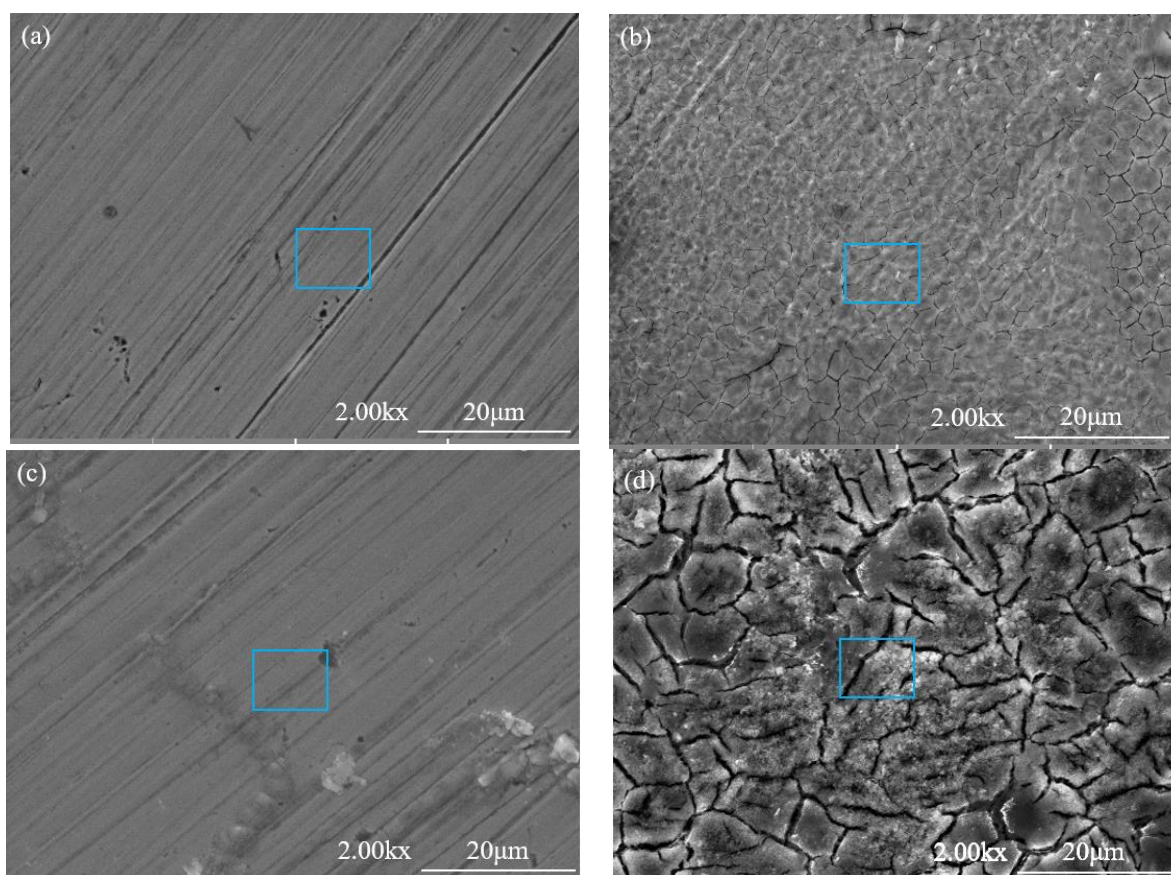


**Figure 11.** SEM images of the inside and outside the crevices of P110 steel under 0 MPa and 400 MPa applied stresses after immersion in the test solution for 12 h

The application of stress accelerates the anode dissolution process in the crevice and promotes the corrosion rate in the crevices, which reduces the Fe content in the P110 steel crevices.

**Table 5.** EDS data of P110 steel inside and outside the crevice after soaking in the simulated solution for 12 h under stresses of 0 MPa and 400 MPa

Element(wt.%)	0MPa(outside)	0MPa(inside)	400MPa(outside)	400MPa(inside)
C	4.12	9.84	5.98	6.63
Na	0.02	0.81	0.12	1.16
Ca	0.01	0.15	0.10	0.23
Cr	0.79	1.40	0.79	3.39
MO	0.40	0.42	0.40	0.50
Fe	94.66	78.38	92.62	64.29

#### 4. DISCUSSION

The crevice corrosion behavior of P110 steel in the simulated solution can be explained by the oxygen differential cell[41] and autocatalytic process[16]. In the initial stage of corrosion, the anodic dissolution reaction and cathodic reduction reaction simultaneously occur on the entire metal surface, as the formula (1) and (2) showed[42], which results in the same corrosive medium and no significant potential difference between inside and outside the crevice.

Anodic dissolution reaction:

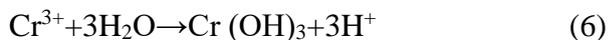
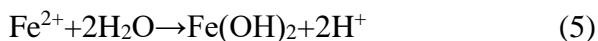


Cathodic reduction reaction:



However, when the reaction on the metal surface continues, the crevice itself limits the supplementation of the cathode reactant ( $\text{O}_2$ ), and the  $\text{O}_2$  content in the crevice rapidly decreases, which inhibits the cathodic reduction reaction in the crevice[43], so the anodic dissolution reaction becomes the main reaction in the crevice. The experiment does not occur under closed conditions.  $\text{O}_2$  is more easily supplemented outside the crevice than inside the crevice, and the cathode reaction continues outside the crevice. As shown in Fig. 4, the P110 steel in the crevice acts as the anode due to the depletion of  $\text{O}_2$ , and the open circuit potential decreases. The P110 steel out of the crevice acts as the site of cathodic reaction, and the open circuit potential increases. This is similar to the results of Li et al. study on N80 crevice corrosion[18]. Hence, a differential aeration cell has been built up between the crevice and the external surface. Due to the macroscopic separation of the cathode and the anode, the uneven distribution of the electrochemical reaction on the metal surface is the main reason for corrosion on the P110 steel. As the corrosion reaction continues, the metal in the crevice is dissolved by the anode reaction, and increasingly many metal ions ( $\text{Fe}^{2+}$ ,  $\text{Cr}^{3+}$ ) accumulate in the crevice. To balance the microenvironment,  $\text{Cl}^-$  ions migrated to the crevice and combined with the metal ions. It was suggested[44] that in order to remain electrically neutral,  $\text{Cl}^-$  will gradually migrate into the crevice, which leads to an increase in the concentration of  $\text{Cl}^-$  within the crevice. As the concentration of  $\text{Cl}^-$ [45] increases, the corrosion potential of the steel shifts in a negative direction, and  $\text{Cl}^-$  participates

in the anodic dissolution process of the steel[46]. The pH value in the crevice decreases with the hydrolysis of chlorides [41], which accelerates the metal dissolution rate, as shown in Equations (4) and (5). The cathodic reaction that occurs on the external surface is also accelerated, which results in a protective effect on the external surface.



$\text{H}^+$  produced by hydrolysis decreases the pH[47] of the corrosive medium in the crevices. Acidification of corrosive media and enrichment of  $\text{Cl}^-$  accelerate the rate of metal dissolution in the crevices. In addition, the solid products produced by the hydrolysis reaction block the crevices. As corrosion progresses, the difference between the environment inside and outside the crevices expands, and the dissolution rate of metal in the crevice accelerates the generation of more metal ions. Repeatedly, the crevice corrosion process of P110 steel under simulated solution conditions has autocatalytic properties and causes more severe crevice corrosion[48]. When the crevice and stress coexist, the electrochemical test results show that different stresses have different promotion effects on crevice corrosion both outside (cathode) and inside the crevice (anode) of P110 steel. Outside the crevice, with the increase in applied stress, the corrosion tendency and corrosion rate of the outside of the crevice increase to varying degrees. Gutman[49] believed that there was an interaction between stress and electrochemistry, and the applied stress made the metal's potential shift in the negative direction. Since the cathodic reaction outside the crevice is the main reaction, the cathodic reaction rate determines the corrosion rate outside the crevice. Li[50] et al. found that the applied stress energy affected the reaction rate of the metal cathodic hydrogen evolution reaction, and the electrochemical potential of the stress weakening hydrogen decreased the activation barrier of the  $\text{H}^+$  reactant discharge and increased the cathodic hydrogen evolution reaction rate. Bao[51] et al. found that with increasing stress, the  $\text{HCO}_3^-$  electrochemical potential adsorbed on the surface of the metal decreased, which increased the electrochemical reaction rate of the cathodic reduction process and accelerated the corrosion process of the metal. In the crevice, the polarization curve and EIS plot show that the applied stress promotes the anodic dissolution rate of the metal and deepens its corrosion behavior. The applied stress makes the metal surface produce stress-strain energy and activation, metals are prone to localized corrosion, dislocation slip is produced, and the metal anodic dissolution process is accelerated[52]. In addition, from the SEM images of different applied stresses, with the increase in applied stresses, more cracks are produced by the corrosion products on the metal surface in the crevice. Gao[53] showed that the corrosion product film on the surface of low carbon steel became looser with increasing applied stress. Zhang[54] also found that stress could change the structure of metal corrosion products, and a higher applied stress corresponds to a more porous corrosion product film. Therefore, the applied stress results in more cracks in the corrosion products and increases the corrosion reaction rate of the metal in the crevice.

This experiment shows that crevice corrosion of P110 steel can be observed in the simulated solution, and there are significant differences between inside and outside of the crevice, and the serious crevice corrosion causes defects on the metal surface. When stresses are applied to the P110 steel, they preferentially destroy the corrosion products, and the barrier effect of the corrosion products is reduced. With the increase in applied stress, the corrosion products becomes chapped, and the dissolution of metal

is accelerated. Simultaneously, the concentrated stress causes an uneven distribution of applied stress on the metal surface, which leads to corrosion cells on the metal surface, induces localized corrosion and crack formation[55], and promotes the development of crevice corrosion of P110 steel. In summary, crevices and stresses have a synergistic effect on the corrosion behavior of P110 in a simulated solution.

## 5. CONCLUSION

In this paper, the effect of crevice-stress synergy on the corrosion behavior of P110 steel in simulated oil and gas field solutions was studied. Based on these results, the following conclusions are drawn:

1. Once the sealing of P110 pipeline steel is destroyed, it will suffer serious crevice corrosion in the simulated solution. The metal in the crevice acts as the anode, but that out of the crevice provides a site for the cathodic reaction. Therefore, the P110 steel in the crevice suffers serious corrosion, and a mass of corrosion products can be observed in the crevice.

2. Stress has a certain role in promoting the anode and cathode reaction process for crevice corrosion, which negatively shifts the corrosion potential of the P110 steel. The crevice corrosion rate of P110 steel inside and outside the crevice was accelerated by applied stress, because the barrier effect of corrosion products is reduced by the applied stress.

## References

1. Y.Z. Li, X. Wang and G.A. Zhang, *Corros. Sci.*, 163 (2020) 108290.1-108290.13.
2. Y.Q. Song, C.W. Du, X. Zhang and X. Li, *Acta Metall. Sinica*, 45 (2009) 1130-1134.
3. J. Guo, J. liu, Q. Hu and F. Huang, *Corrosion Science and Protection Technology*, 28 (2016) 6.
4. Y.H. Lee, Z. Takehara and S. Yoshizawa, *Corros. Sci.*, 21 (1981) 391-397.
5. X. Meng, Z. Lin and F. Wang, *Mater. Des.*, 51 (2013) 683-687.
6. D.A. Horner, B.J. Connolly, S. Zhou, L. Crocker and A. Turnbull, *Corros. Sci.*, 53 (2011) 3466-3485.
7. J. Hahm and S. J. Sibener, *Appl. Surf. Sci.*, 161 (2000) 375-384.
8. X. Tang and Y.F. Cheng, *Electrochim. Acta*, 54 (2009) 1499-1505.
9. J. Torkkeli, T. Saukkonen and H. Hanninen, *Corros. Sci.*, 96 (2015) 14-22.
10. S.C. Yoo, K.J. Choi, T. Kim, S.H. Kim, J.Y. Kim and J.H. Kim, *Corros. Sci.*, 111 (2016) 39-51.
11. A. Turnbull, L.N. McCartney and S. Zhou, *Corros. Sci.*, 48 (2006) 2084-2105.
12. L.K. Zhu, Y. Yu, L.J. Qiao and A.A. Volinsky, *Corros. Sci.*, 77 (2013) 360-368.
13. B.T. Lu, Z.K. Chen, J.L. Luo, B.M. Patchett and Z.H. Xu, *Electrochim. Acta*, 50 (2005) 1391-1403.
14. G.A. Zhang and Y.F. Cheng, *Electrochim. Acta*, 55 (2009) 316-324.
15. S.L. Wang, Y.Z. Jing, C.Q. Ren, L. Liu and M.Y. Bao, *Materials Protection*, 52 (2019) 13-19.
16. J. Mu, Y.Z. Li and X. Wang, *Corros. Sci.*, 182 (2021) 109310.
17. G.Y. Zhu, Y.Y. Li, B.S. Hou, Q.H. Zhang and G.A. Zhang, *Journal of Materials Science & Technology*, 88 (2021) 79-89.
18. Y.Z. Li, X.P. Guo and G.A. Zhang, *Corros. Sci.*, 123 (2017) 228-242.

19. C. Torresa, R. Johnsen and M. Iannuzziab, *Corros. Sci.*, 178 (2021) 109053.
20. Y. Li, Z. Wang, M. Zhao and G. Zhang, *Ind. Eng. Chem. Res.*, 57 (2018) 8718–8728.
21. T. Wu, Y.X. Liu, J. Qin, Y. Wang, S.G. Ye, X.G. Feng and S.L. Chen, *Int. J. Electrochem. Sci.*, 15 (2020) 8375-8385.
22. J.Q. Xue, Y. Zhang, C.B. Bin, L.H. Yu and C.X. Yi, *Corrosion Science and Protection Technology*, 29 (2017) 34-40.
23. G.A. Zhang and Y.F. Cheng, *Corros. Sci.*, 51 (2009) 1589-1595.
24. Z.X. Yao, S. Jiang, G W, L.M. Yin, D.P. Jiang and Z.W. Zhang, *Int. J. Electrochem. Sci.*, 14 (2019) 2672-682.
25. X.Z. Wang, H. Luo and J.L. Luo, *Electrochim. Acta*, 293 (2019) 60-77.
26. H. Luo, X. Wang, C. Dong, K. Xiao and X. Li, *Corros. Sci.*, 124 (2017) 178-192.
27. Z. Cui, S. Chen, Y. Dou, S. Han, L. Wang, C. Man, X. Wang, S. Chen, Y.F. Cheng and X. Li, *Corros. Sci.*, 150 (2019) 218-234.
28. J.D. Henderson, N. Ebrahimi, V. Dehnavi, M. Guo, D.W. Shoesmith and J.J. Noel, *Electrochim. Acta*, 283 (2018) 1600-1608.
29. J.E.G. González, A.F.J.H. Santana and J.C. Mirza-Rosca, *Corros. Sci.*, 40 (1998) 2141-2154.
30. M.X. Guo, L. Xiao, R.T Jun, P. Chen and Y.W. Zhen, *Int. J. Electrochem. Sci.*, 16 (2021) 210457.
31. J.B. Li, X. Hou, M.S. Zheng and J.W. Zhu, *Int. J. Electrochem. Sci.*, 2 (2007) 607.
32. W.J. Yang, P. Yang, X.M. Li and W.L. Feng, *Mater. Corros.*, 63 (2012) 401.
33. F.Q. Bi, B. Zhou, Y.X. Yin and S. Yan, *Chemical Engineering & Machinery*, 45 (2018) 429-433.
34. A. Singh, K.R. Ansari and M.A. Quraishib, *Int. J. Hydrogen Energy*, 46 (2020) 25398-25408.
35. Y.Z. Li, N. Xu, X.P. Guo and G.A. Zhang, *Corros. Sci.*, 123 (2018) 9-22.
36. F. Almuaili, S. McDonald, P. Withers and A. Cook, *Corros. Sci.*, 125 (2017) 12-19.
37. M.Y. Bao, C.Q. Ren, M.Y. Lei, A. Singh and X.Y Guo, *Corros. Sci.*, 112 (2016) 585-595.
38. F.A. Chen, R.Z. Xie, B. He, Z.W. Chen, X.L. Bai and P.J. Han, *Int. J. Electrochem. Sci.*, 16 (2021) 150878.
39. Y.Z. Pan, Y. Wang, F.Q. Guo, T. H. Zhang, K.J. Matsuda, D.T. Wu, Y.A. Zhang and Y. Zou, *J. Mater. Res. Technol*, 15 (2021) 1130-1144.
40. Z. Bin, C. Yi, A. Fang, G Peng, L. Lin, M. Fan and S. Hong, *Corrosion Science and Protection Technology*, 31 (2019) 5.
41. P. He, D.H. Suo, W.B. Wu, L.Q. Yin, W. Dai, B. G. Shang, Y.Y. Liu, Y.T. Sun, Y. M. Jiang and J. Li, *J. Mater. Res. Technol*, 19 (2022) 101-120.
42. B. Zhao, H.X. Wan, Y.Y. Peng, C. Liu, J. Li and B.N. Shou, *Int. J. Electrochem. Sci.*, 16 (2021) 150808.
43. L.B. Niu, K. Okano, S. Izumi, K. Shiokawa, M. Yamashita and Y. Sakai, *Corros. Sci.*, 132 (2018) 284-292.
44. Q. Hu, X.P. Guo, G.A. Zhang and Z. Dong, *Mater. Corros.*, 63 (2012) 720-728.
45. N. Zhang, D. Zeng, G. Xiao, J. Shang, Y. Liu, D. Long, Q. He and A. Singh, *J. Nat. Gas Sci. Eng.*, 30 (2016) 444-454.
46. R.J. Chin and K. Nobe, *J. Electrochem. Soc.*, 119 (1972) 1457-1461.
47. Z. Y. Liu, X. G. Li and Y. F. Cheng, *Corros. Sci.*, 55 (2012) 54-60.
48. J.W. Oldfield and W.H. Sutton, *Br. Corros. J.*, 13 (1978) 13-22.
49. E.M. Gutman, *Corros. Sci.*, 49 (2007) 2289-2302.
50. D.G. Li, Y.R. Feng, Q.Z. Bai and M.S. Sheng, *Acta Chim. Sinica*, 65 (2007) 7.
51. M.Y. Bao, J.J. Xiong, C. Liu, J. Zhang, C.C. Qi and K.X. Miao, *Natural gas and oil*, 38 (2020) 88-95.
52. M.M.H. Jr, *Corros. Sci.*, 51 (2009) 225-233.
53. K. Gao, D. Li, X. Pang and S. Yang, *Corros. Sci.*, 52 (2010) 3428-3434.
54. J. Zhang, Q. Hu, F. Huang, Z.Y. Cheng and J.T. Guo, *Anti-Corros. Methods Mater.*, 62 (2015) 103-108.

55. H.Q. Yang, Q. Zhang, S.S. Tu, Y. Wang, Y.M. Li and Y. Huang, *Corros. Sci.*, 110 (2016) 1-14.

© 2022 The Authors. Published by ESG ([www.electrochemsci.org](http://www.electrochemsci.org)). This article is an open access article distributed under the terms and conditions of the Creative Commons Attribution license (<http://creativecommons.org/licenses/by/4.0/>).